Near-surface structure of low-energy-argon-bombarded Si(100)

L. J. Huang and W. M. Lau

*Surface Science Western and Department of Materials Engineering, University of Western Ontario,
London, Ontario, Canada N6A 5B7*

H. T. Tang, W. N. Lennard, I. V. Mitchell, and P. J. Schultz

Department of Physics, University of Western Ontario, London, Ontario, Canada N6A 3K7

M. Kasrai

Department of Chemistry, University of Western Ontario, London, Ontario, Canada N6A 5B7

The near-surface structure of low-energy- (0.5–1.5 keV) Ar-bombarded Si(100) has been studied using high-resolution x-ray-absorption near-edge structure spectroscopy and extended x-ray-absorption fine-structure spectroscopy with synchrotron radiation, medium-energy ion scattering, variable-energy positron-annihilation spectroscopy, and angle-resolved x-ray photoemission spectroscopy. The ion-induced defect structure for silicon, and the structure and distribution of incorporated Ar and silicon carbide formed during the dynamic mixing process are directly and nondestructively measured and depth profiled in the subnanometer scale. The results indicated that no Ar bubble was formed at moderate bombardment fluences ($\sim 10^{16}$/cm^2) and that epitaxial recrystallization could be achieved by postbombardment vacuum annealing at 700 °C for 30 min.

I. INTRODUCTION

Ar ion beams are widely used for surface cleaning and ion-assisted dry etching of semiconductors.[1] They are also often used in ion-assisted deposition[2] and sputter depth profiling techniques that are available with many analytical instruments, e.g., Auger electron (AES) and x-ray photoemission (XPS) spectrometers.[3] The advantages of using Ar ion beams for these particular applications arise from their chemical inertness and high sputtering yield, e.g., the sputtering yield[4] for 1 keV Ar ions on silicon is about 0.8 to 1.0. However, the ion bombardment process has the inherent drawback that the ion-solid interaction usually produces a distorted or disordered surface/near-surface layer, depending on the bombarding energy and fluence. Although the ion-induced damage can be decreased by lowering the ion energy, such a gain is offset by a substantial decrease in the sputtering yield. In addition, the bombardment/sputtering process will also lead to dynamic ion mixing and Ar retention in the near-surface layer, which could be detrimental for particular applications. Many research efforts are therefore directed towards the understanding of the surface and near-surface structure following energetic Ar bombardment and the effects of the subsequent thermal processing on the bombarded surface and near-surface structure.[5-14] Nevertheless, a clear picture of the near-surface structure has not yet emerged via direct experimental evidence. For example, measurements of the depth distribution of incorporated Ar and the associated recrystallization of silicon near the surface after low-energy (less than a few keV) Ar ion bombardment

are yet to be performed.

Bean *et al.*[5] were among the first to systematically investigate the near-surface structure of silicon after Ar bombardment. They successfully identified temperature effects on the Ar retention rate for 1 keV Ar bombardment using the Rutherford backscattering (RBS) technique. Ar retention was found only when the bombarded silicon substrate was maintained above room temperature. However, the relatively poor depth resolution (e.g., ~ 160 Å for 1.6 MeV He$^+$ in the RBS/channeling low-exit-angle mode) precluded a determination of the depth distribution of the Ar incorporated into the silicon. Using medium-energy ion scattering (MEIS) spectroscopy, Al-Bayati *et al.*[9] achieved a depth resolution of 3 Å and measured the depth distribution of displaced silicon atoms with 60–510 eV Ar$^+$ bombardment. They reported the formation of an amorphous layer in the near-surface region of silicon for Ar ion fluences exceeding 5×10^{15}/cm^2 at ion energies greater than 100 eV. Nevertheless, a true depth distribution of the displaced silicon and incorporated Ar was not obtained due to the limited mass resolution in the experimental setup.[9]

For the minimization of defects in a damaged near-surface layer arising from Ar ion bombardment, one approach is to perform the bombardment at an elevated temperature. When the Ar ion fluence is low, the bombardment-induced defects are dominated by divacancies which can be annealed out at $T \sim 300$ °C. Consequently, a significant decrease in the damage is observed at a bombardment temperature above 400 °C for ion fluences below 5×10^{15}/cm^2.[5-9] For higher ion fluences, however, elevating the bombardment temperature will

result in the formation of extended defects in the subsurface region caused by thermally enhanced point defect migration, combination, and stabilization. For ion fluences exceeding $10^{18}/cm^2$, pronounced disordering such as dislocations and Ar bubbles was indeed observed.[5] Such an observation was confirmed by Ar thermal desorption spectra measured by Filius *et al.*,[12] who observed multiple argon cluster desorption peaks near $T = 600\,°C$ for bombardment fluences above $10^{17}/cm^2$. The increase of the Ar incorporation probability at larger bombarding fluences was also identified by several authors.[5,12] The extended defects thus formed are located in the silicon subsurface and may not be detected by surface-sensitive techniques, e.g., low-energy electron diffraction (LEED) or AES. Another approach to the recrystallization of the damaged silicon near-surface layer was through postannealing under vacuum. One of the advantages for vacuum postannealing when compared to that by bombardment at an elevated temperature is that it occurs without continuous delivering of Ar into the substrate and the incorporated Ar will be annealed out consistently. Recent data[13] have shown that migration and release of Ar occurs at a temperature as low as $250\,°C$, which is probably associated with the dissociation of vacancy-type defects. Hence, postannealing is unlikely to induce the formation of extended defects such as Ar clustering. The postannealing approach has been proposed[5,9] as the preferred method for obtaining a recrystallized silicon near-surface layer. It should be mentioned that controllable recrystallization through high-energy ion beams[15] has drawn much attention recently. However, this technique is not suitable for recrystallization in nanometer scale and in the near-surface or subsurface region.

Since Ar ion bombardment of silicon is a dynamic process, the near-surface structure of silicon after the bombardment also depends on the surface cleaning before the bombardment. For example, if the silicon surface is contaminated with carbon, a thin layer of SiC arising from ion mixing will be formed in the near-surface region during the bombardment.[16–18] In fact, in most of the relevant applications, Ar bombardment is performed by backfilling the vacuum chamber. Thus it is difficult to completely avoid contamination by adventitious hydrocarbons. The SiC formed in this way usually has a stable structure which is resistant to desorption by thermal annealing. However, quantitative and nondestructive measurements of such a SiC structure have not been reported to date.

In this paper, we use mass-resolved MEIS, high-resolution x-ray-absorption near-edge structure (XANES) spectroscopy, and extended x-ray-absorption fine-structure (EXAFS) spectroscopy with synchrotron radiation, XPS, and variable-energy positron-annihilation spectroscopy to measure directly and nondestructively the near-surface structure of single-crystal Si(100) bombarded by low-energy (0.5–1.5 keV) Ar ions. The silicon defect structure and its recrystallization, the structure of incorporated Ar and its redistribution upon post-annealing, and the structure and distribution of the ion-induced silicon carbide have been quantified and depth profiled on the subnanometer scale.

II. EXPERIMENT

A. Sample preparation

Single-crystal Si(100) samples were phosphorus doped to a concentration of $10^{16}/cm^3$. The defect density in the crystal was less than $2 \times 10^3/cm^3$, according to the manufacturer. Before Ar bombardment, all the samples were cleaned first by ultraviolet (uv) ozone oxidation to remove adventitious hydrocarbons, and second with 5% hydrofluoric acid to remove the oxides and produce a hydrogen-terminated surface.[19] The ion bombardments were all performed in an XPS-equipped ultrahigh vacuum analytical chamber. The chamber vacuum before backfilling with pure Ar gas was about 5×10^{-9} Torr. Ar ion beams with energies in the range 0.5–1.5 keV were extracted from a scanning Leybold ion gun through a needle valve and a differential pump, while the pressure of the chamber was maintained at 2×10^{-7} Torr. The ion fluence was measured by a Faraday cup. An ion fluence of $10^{16}/cm^2$ over a 2×2 mm^2 sample area was delivered in about 110 s. Two bombardment angles ($0°$ and $55°$) between the sample normal and the ion beam were chosen to study the angle dependence of Ar and silicon displacement distributions. *In situ* XPS was carried out before and after the ion bombardments. To protect the surface from air oxidation during sample transfer, the as-bombarded samples were immediately transferred into an uv-ozone oxidation reaction chamber and capped with ~ 10 Å SiO_2.[20] The reaction initiated by the uv photons was also expected to remove adventitious surface hydrocarbons during the sample transfer. Although the cap consumed the top 0.5 nm of the bombarded Si layer, the bulk of the damage layer (>40 Å) would be protected from reaction with the ambient air. A HF-cleaned Si(100) single crystal was also capped with the ozone oxide using the same process as a reference for all the measurements. All postbombardment anneals were performed in a vacuum chamber which was maintained at 2×10^{-9} Torr, and the annealing time was fixed at 15 min.

B. Characterization

The MEIS measurements were performed using the 1.7 MV Tandetron accelerator at the University of Western Ontario. A collimated beam of $^4He^+$ ions incident on the samples at 250 keV was elastically scattered and analyzed with regard to scattering angle and energy via a high-resolution toroidal electrostatic analyzer. The spectra were collected in the double alignment configuration. The scattering angle between the incoming channeling string and the outgoing (scattering) ion direction was $90°$. The energy resolution for all the MEIS data was about 0.2%, which is equivalent to a depth resolution of ~ 4 Å for silicon. Different channeling and blocking axial directions were measured to verify the measured distributions for impurities and silicon displacements in the bombarded samples. For comparison, conventional RBS

with a 1 MeV ^{4}He$^+$ ion beam was also employed to measure some of the samples in this study. The RBS energy resolution was 15 keV, which transforms into an equivalent depth resolution of ~60 Å. XANES and EXAFS spectra were measured at the Canadian Synchrotron Radiation Facility (Aladdin) on the 1 GeV electron storage ring operated by the University of Wisconsin at Madison. The x ray was monochromatized and the photon resolution at 100 eV was ~0.1 eV. The total electron yield (TEY) mode was used for both the XANES and EXAFS measurements. In order to eliminate the unrelated structures in the measurements, all the TEY spectra were normalized to the TEY signal simultaneously recorded from a gold mesh reference monitor. XPS and angle-resolved XPS (ARXPS) measurements were performed using a Surface Science Instrument SSX-100 spectrometer with a monochromatic Al $K\alpha$ x-ray spot size of 300 μm and a pass energy of 25 eV. Variable-energy positron-annihilation measurements were done at the Positron Beam Laboratory at the University of Western Ontario. Detailed descriptions of the experimental systems and the relevant experimentation can be found in previous publications.[21−25]

III. RESULTS AND DISCUSSION

A. Characterization of the cap layer

The major concern for *ex situ* measurements of the near-surface structure of silicon after low-energy (less than a few keV) Ar ion bombardment is the instability of the surface and/or near-surface during sample transfer since the thickness of the defect layer formed during the bombardment is expected to be of the order of a few nanometers. To maintain a consistent surface condition, all samples in this study were immediately capped with ozone oxide after the bombardment. The ozone oxide was formed in an uv-light-induced ozone reaction chamber described previously.[25] The thickness of the oxides, t_{SiO_2}, was calculated from the measured XPS photoemission intensities for oxide, I_{SiO_2}, and silicon I_{Si}, signal in the Si $2p$ spectra (Fig. 1), respectively, using

$$t_{SiO_2} = \lambda_{SiO_2} \cos\theta \ln\left(\frac{I_{SiO_2}\rho_{Si}\lambda_{Si}}{I_{Si}\rho_{SiO_2}\lambda_{SiO_2}} + 1\right), \quad (3.1)$$

where λ is the inelastic mean free path[26] (IMFP) of the photoelectrons and θ is the experimental polar angle (55°). The fitting positions for suboxide peaks shown in Fig. 1 were the same as those identified in the literature[27] and for clarity only one fitted peak for each of the suboxide is shown. The calculations showed that ~5 Å silicon on the very top of the samples had been consumed. If the oxide thickness calculation included the contribution of the suboxide, the difference of the oxide cap thickness between HF-etched single-crystal Si(100) [Fig. 1(a)] and the bombarded sample [Fig. 1(b)] was ~3 Å, and hence the difference of the thickness for the consumed silicon was ~1.3 Å. The ozone oxide was found to be very stable, i.e., the change of the oxide thickness measured by
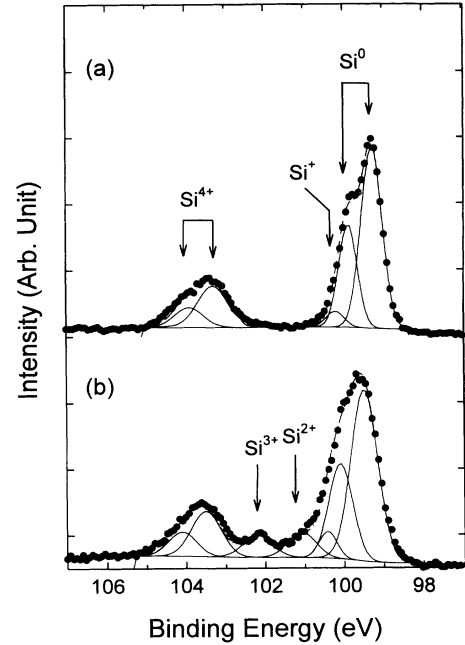

FIG. 1. XPS spectra for (a) HF-etched Si(100) and (b) 1 keV argon-ion-bombarded Si(100) to an ion fluence of 1×10^{16}/cm^2. Both samples were capped with ozone oxide.

XPS over a period of six months was within the measurement error (<1 Å). Since the uv oxidation is conducted at ambient temperature, the bulk of the defect structure is not expected to be modified during the capping process. To verify that the uv ozone process does not induce the desorption of impurities inside the defective layer, XPS was used to measure the photoemission intensity ratio of Ar/Si before and after the capping process for the Ar-bombarded samples. It was found that the change of the ratio was within the measurement error ($\pm5\%$).

B. Near-surface structure after argon bombardment

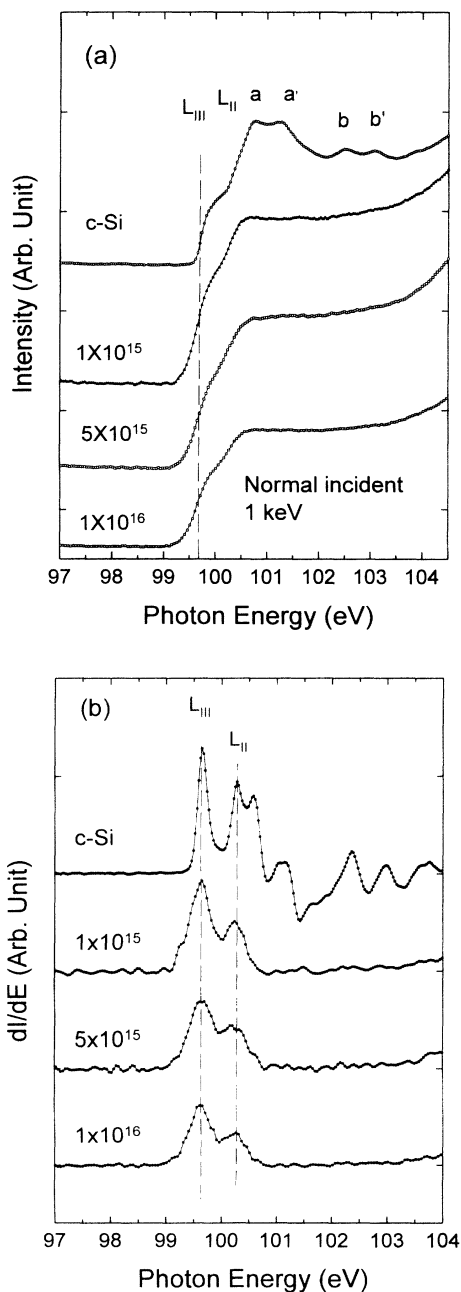Figure 2 shows the Si $L_{II,III}$ XANES spectra for a HF-etched Si(100) and 1 keV Ar-ion-bombarded Si(100) to different ion fluences as labeled in the figure, and Fig. 2(b) is the first order derivative of the Si $L_{II,III}$ XANES spectra for the corresponding spectra shown in Fig. 2(a). XANES yields a direct measurement of the near-surface structure under the oxide cap since the absorption edge for SiO$_2$, which is not shown in this figure, is ~5 eV above the silicon edge. Comparing the spectra in Fig. 2(b) and Fig. 2(a), the Si L_{III} and L_{II} absorption edges for all the samples are resolved and the derivative spectra provide much better resolution visually. The peaks a and b in Fig. 2 are associated with maxima in the unoccupied density of states and their replicas, a' and b', are due to the spin-orbit splitting (0.61 eV).[28−31] These peaks have been identified as evidence of a prevailing long range order in the sample. The edge jump (threshold) in the above spectra is known as the transition at the Δ_1 minimum of the silicon band structure and therefore its

position could be an indication of the position of the conduction band minimum (CBM). Such a position can be seen more clearly in Fig. 2(b), where the $2p_{3/2}$ and $2p_{1/2}$ to $3s$ transitions are well resolved and labeled by L_{III} and L_{II}. The photon energy position for L_{III} is at 99.7 eV, which agrees well with the value previously reported.[32,33] From the XANES data (Fig. 2), it was evident that a disordered near-surface layer had been induced after bombardment to an ion fluence of $10^{15}/cm^2$ since all the peaks above the edge shown in the spectrum for the c-Si

were absent. Evidence for the formation of the disordered near-surface structure could also be seen in the spectra shown in Fig. 2(b) where the peaks corresponding to the L_{III} and L_{II} edges for the bombarded samples were much broader ($\sim$ 2.5 times) than those for the c-Si. The peak broadening resulted in a tail towards the valence band maximum (VBM). For the sample bombarded to an ion fluence of $10^{16}/cm^2$, such a tail extended about 0.5 eV below the CBM which was approximately in the middle of the band gap. The observed x-ray-absorption intensities below the CBM suggest a high density of surface states across the band gap, which was characteristic of amorphous silicon.

Compared to the XANES for the Si L edge, XANES for the Si K edge is more bulk sensitive. Nevertheless, the measured results (Fig. 3) show a substantial decrease of the bound to bound dipole transition for the bombarded sample. This dipole transition is due to the Si $1s$ to the projected unoccupied states of Si p character in the conduction band at the Si site.[34] In other words, the bombardment induced a decrease in the population of the Si p holes. The Fourier transform (FT) of the corresponding EXAFS data shown in Fig. 3, however, indicated only marginal changes in the shoulders of the FT magnitudes for the first three shells. Further calculations of the Si-Si bond lengths from the FT data were based on the experimental phase function $\Phi(k)=\sin(2kr+\rho_{a,b})$, where k is the photoelectron wave vector and $\rho_{a,b}$ is the theoretical atomic pair phase function for a Si-Si absorber-scatter pair.[35] The measured absorption coefficient $\chi(k)$
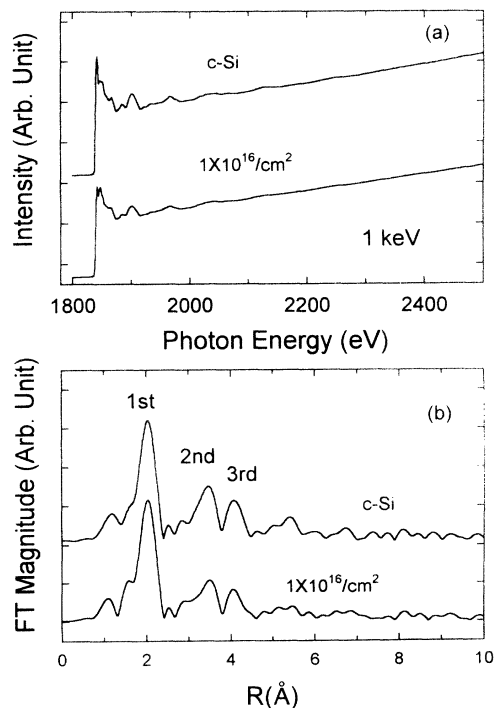

FIG. 2. (a) Si $L_{II,III}$ XANES spectra for HF-etched Si(100) and 1 keV argon-ion-bombarded Si(100) to different ion fluences as labeled in the figure. (b) The first order derivative of the Si $L_{II,III}$ XANES spectra for the corresponding spectra shown in Fig. 2(a).

FIG. 3. (a) The Si K EXAFS spectra for HF-etched and 1 keV Ar-bombarded Si(100) to an ion fluence of $1\times10^{16}/cm^2$. Both of the samples were capped with ozone oxide. (b) The Fourier transformation of the corresponding EXAFS data shown in (a).

was weighted with k^n (n=1,2,3) for different regions of the data in k space.[35] By filtering and backtransforming, the FT data indicated that the first shell nearest Si-Si interatomic distances for both the c-Si and the bombarded sample were identical (r= 2.35 Å). The distances calculated from the second and third shells using a k^2 weighting showed a slight expansion $\sim$ 6% (the calculation error is $\sim$ 2%) for the bombarded sample as compared to those for c-Si. The small changes measured in the present experiment are substantially different from that measured from bulk amorphous Si.[36] This is probably because the detection depth of Si K edge measurement is much deeper than the depth of the bombardment-induced amorphous layer. The strong substrate signal suppressed the signal from the bombarded layer. Another evidence of a much deeper detection depth for the K edge measurement comes from the fact that the SiO_2 signal almost could not be identified in the spectra.

C. Damage depth profiling and argon retention measured by MEIS

Quantitative measurements of the Ar-bombarded silicon near-surface structure were performed by MEIS. Figure 4(a) shows the MEIS spectra for the samples bombarded by 0.5 keV and 1 keV Ar ions, respectively, both to an ion fluence of $10^{16}/cm^2$ and at a bombardment angle of 0°. The spectra were collected in a double alignment configuration in which $\langle 111 \rangle$ was chosen as the incoming ion channeling direction and the outgoing ions were collected at a scattering angle of 90° along the $\langle \bar{1}\,\bar{1}2 \rangle$ string direction. The spectrum for a silicon single-crystal sample is also included for comparison. It can be observed from the figure that the intensities for the channeling spectra and the random spectra reached the same height, which suggests that the bombarded near-surface layer had been completely amorphized (disordered) at this ion fluence; this observation agrees with the XANES data (Fig. 2) and those reported in the literature.[5,9] In these spectra, the silicon and Ar surface energy positions (at 187.62 keV and 204.55 keV, respectively) are well separated, which makes it possible to obtain a quantitative depth profile of the respective silicon displacement and Ar retention at the near-surface layer of the bombarded samples. The number of displaced silicon atoms per unit area, including atoms on an ideal surface layer $(Nt)_{Si}$, can be calculated from the measured area A of the surface peaks in the spectra by[37]

$$(Nt)_{Si} = (A/\sigma\Omega Q)\cos\theta, \tag{3.2}$$

where σ is the elastic scattering cross section, Ω is the detector solid angle, Q is the integrated number of $^4He^+$ ions, and θ is the angle between the direction of the $^4He^+$ beam and the sample normal. Alternatively, $(Nt)_{Si}$ can be calculated[37] from the measured difference in energy of detected ions backscattered at the surface and from the interface, ΔE,
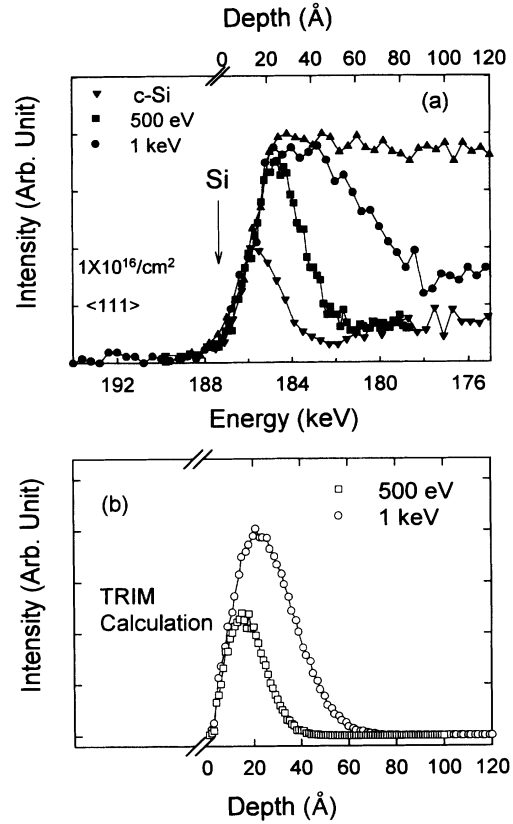
$$(Nt)_{Si} = \Delta E/[\epsilon], \tag{3.3}$$

FIG. 4. (a) MEIS spectra showing the silicon surface peaks for 0.5 keV and 1 keV bombarded Si(100), both to an ion fluence of $1 \times 10^{16}/cm^2$. The spectrum for a HF-etched Si(100) single crystal is also included for reference. All the samples were capped with ozone oxide silicon. (b) TRIM calculation of the silicon displacement depth distribution for 0.5 keV and 1 keV argon-bombarded silicon.

where $[\epsilon]$ is the stopping cross section. For the data shown in Fig. 4(a), we found that the relative difference between the values calculated using Eqs. (3.2) and (3.3) was about 1%. The calculated areal densities for the 0.5 keV and 1 keV Ar-bombarded samples [Fig. 4(a)] are $1.45\times10^{16}/cm^2$ and $3.54\times10^{16}/cm^2$, respectively. By subtracting the ideal silicon surface peak areal density $(1.27\times10^{15}/cm^2)$ from that of the sample without bombardment $(9.84\times10^{15}/cm^2)$, we deduced that the contribution of the cap layer to the measured areal density was $8.57\times10^{15}/cm^2$. This value agrees well with that of a 10 Å thin oxide on a silicon single crystal measured by RBS using incident 0.8 MeV $^4He^+$ ions.[38] Consequently, the corrected average areal densities for the 0.5 keV and 1 keV Ar-bombarded samples were $5.93\times10^{15}/cm^2$ and $2.68\times10^{16}/cm^2$, respectively. Both values are smaller but of the same order of magnitude compared to those in the literature.[9,11,39,40] The projected ranges of the displaced silicon atoms calculated from the measured data [Fig. 4(a)] were 17 Å and 31 Å for 0.5 keV and 1 keV bombardments, respectively. Compared to those from a TRIM simulation[41] shown in Fig. 4(b), the simulated value for 0.5 keV bombardment overestimated the damage depth

while for the 1 keV bombardment the measured and the simulated values agree well with each other. This result is not surprising since the TRIM code was basically written for the simulation of high-energy ion-solid interactions. It should be pointed out that one cannot directly compare the depth scales shown in Figs. 4(a) and 4(b). An amorphous sample was assumed in the simulation [Fig. 4(b)] while the measured depth has to be corrected with respect to the scattering configuration. This observation probably accounts for our measured projected ranges being smaller than those reported in the literature.[9]

Theoretically, for a monoenergetic monoisotopic ion beam, the depth distribution of bombardment-induced defects depends significantly on the bombardment angle. However, in most commercial ion guns, energetic neutrals are not separated from the ion beam. Thus, it is difficult to control precisely the bombardment fluences. To understand the contribution of neutrals in our experiments, MEIS (Fig. 5) was employed to measure the defect and impurity distributions at various bombardment angles. RBS (Fig. 6) was also used for comparison to measure such effects under channeling conditions. In Fig. 5, it can be seen that the energy difference for ions at the surface and at the interface in the spectra collected for both $\langle 110 \rangle$ and $\langle 111 \rangle$ incoming ion channeling strings from the samples bombarded at the bombardment angles of 55° and 0° is approximately the same. The relative difference of the theoretical projected ion energy at these two bombardment angle is, however, ~42%. Hence, the spec-

tra clearly show that energetic neutrals have a significant contribution to the depth distribution of bombardment-induced defects. The areal densities for the displaced silicon atoms and Ar impurities calculated from the spectra shown in Figs. 5 and 6 are given in Table I, where all the data have been calibrated to (i) the scattering configuration and (ii) the contribution of the surface cap layer. The relative error of the numerical results collected at different scattering configurations using MEIS or RBS is within 10%. However, the data measured for displaced silicon atoms from RBS are systematically larger than those from MEIS by ~20%, while those for incorporated Ar are systematically smaller. Since the depth resolution for RBS is approximately 20 times worse than that for MEIS, the error from the RBS measurements is much larger than that from MEIS. The areal density for total incorporated Ar measured by MEIS was about $10^{15}/cm^2$, which agrees with the Ar desorption data measured using a quadrupole mass spectrometer by Filius *et al.*[12]

The Ar retention ratio (total incorporated Ar over total ion fluence) can also be measured from the ion scattering data. Figure 7(a) shows the Ar intensities for 1 keV Ar-ion-bombarded Si(100) to different ion fluences and Fig. 7(b) is the calculated Ar retention ratio. The actual ratio should be smaller than the number given in the figure since the contribution of neutrals is not included. Nevertheless, the value of 0.4 for the low-fluence ($10^{15}/cm^2$) bombardment is lower than that measured from the absorption experiment (~1) by Filius *et al.*[12]
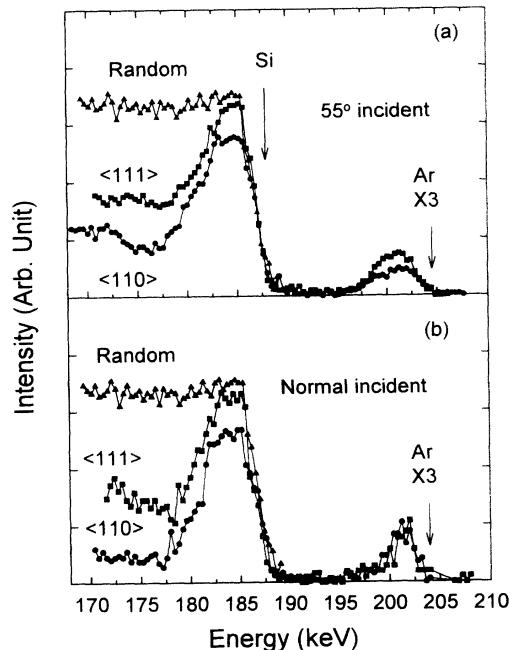

FIG. 5. MEIS spectra for 1 keV argon-bombarded Si(100) samples at different incident angles between the sample normal and the direction of ion beam: (a) 35° and (b) normal incidence. The $\langle 111 \rangle$ and $\langle 110 \rangle$ strings were separately chosen as the incoming channeling direction, and the outgoing ions were collected at a scattering angle of 90° along $\langle \bar{1}\bar{1}2 \rangle$ and $\langle 001 \rangle$ directions, respectively.
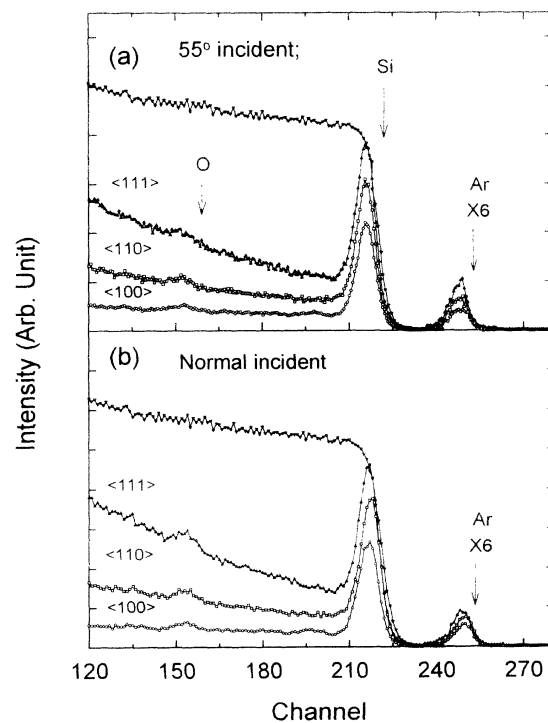

FIG. 6. RBS spectra with 1 MeV $^4He^+$ analytical beam for 1 keV argon-bombarded Si(100) samples at different incidence angles between the sample normal and the direction of ion beam: (a) 35° and (b) normal incidence. The channeling spectra were taken along the three major crystal strings.

TABLE I. Calculated silicon displacement area density and argon intensities from MEIS and RBS spectra for Si(100) bombarded by 1 keV argon beam to an ion fluence of 1×10^{16}/cm^2. The units for all the data in the table, except for the unitless Ar/Si ratio, are 10^{16}/cm^2.

| | | | Incoming ion channeling direction | | |
		Bombardment angle	$\langle 100 \rangle$	$\langle 110 \rangle$	$\langle 111 \rangle$
RBS	Si	55°	4.67	4.70	5.03
		90°	3.61	3.76	3.90
	Ar	55°	0.093	0.095	0.12
		90°	0.067	0.068	0.072
	Ar/Si	55°	0.02	0.02	0.02
		90°	0.02	0.02	0.02
MEIS	Si	55°		3.15	2.99
		90°		2.75	2.68
	Ar	55°		0.11	0.12
		90°		0.13	0.11
	Ar/Si	55°		0.03	0.04
		90°		0.05	0.04

D. Argon depth profiling and argon defect structure

Figure 8 shows MEIS data for the Ar depth profile for samples bombarded to an ion fluence of 10^{16}/cm^2, but at different ion energies. These spectra were collected at a scattering angle of 90° with $\langle 111 \rangle$ and $\langle \bar{1}\,\bar{1}2 \rangle$ as the incom-

ing and outgoing ion channeling directions, respectively. The measured depth profiles [Fig. 8(a)] are compared to those from TRIM simulations [Fig. 8(b)]. By calibrating the measured depth with respect to the scattering configuration, it was found that the projected depths for Ar in the 1 keV and 1.5 keV Ar-bombarded samples were 31
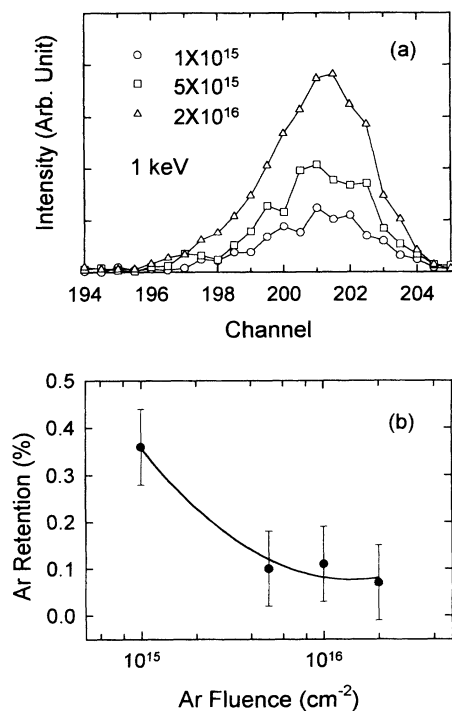

FIG. 7. (a) Argon intensities for 1 keV argon-ion-bombarded Si(100) to different ion fluences. (b) Calculated argon retention ratio for 1 keV argon-bombarded Si(100) to different fluences.
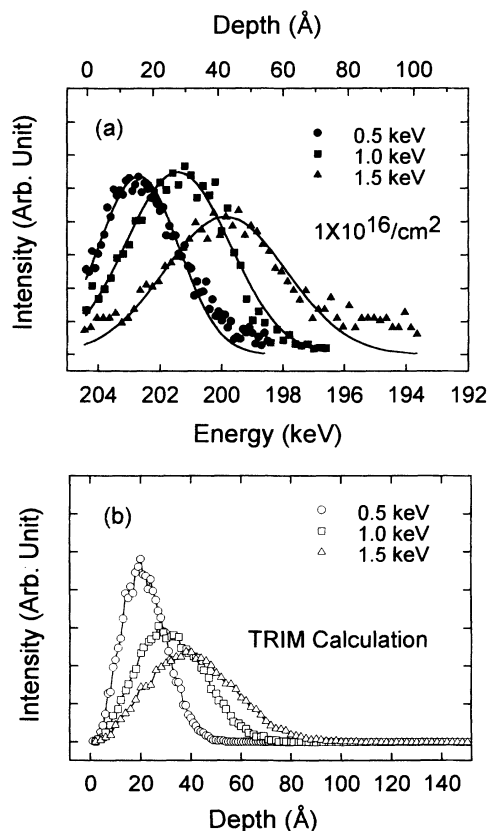

FIG. 8. (a) Argon depth profile by MEIS for different argon ion energies. The ion fluences were 1×10^{16}/cm^2 and the bombardment angle was 0° for all the samples. (b) Argon depth distribution calculated by TRIM.

Å and 45 Å, respectively; both values agreed well with the TRIM simulations. For the projected depth of Ar in the 0.5 keV Ar-bombarded sample, the measured value was 18 Å while the simulation indicated a depth of 22 Å. The results are similar to those of the calculation for displaced silicon atoms discussed above. The areal densities for the Ar incorporated in the 1 keV and 1.5 keV Ar-bombarded samples were found to be the same (1.1 × 10^{15}/cm^2), while the value for that in the 0.5 keV Ar-bombarded sample was 8.3 × 10^{14}/cm^2, a value that is slightly lower than the other two. It was also found that the Ar depth distribution can be approximated by a Gaussian distribution. The solid lines in Fig. 8(a) are the results from fitting using a Gaussian function. At the lower energy (0.5 keV), the distribution is asymmetric. Such a profile suggests saturation or quasisaturation of the Ar impurities in the surface region.

The defect structure of the retained Ar at the near-surface of silicon has drawn a great deal of interest since the chemical affinity between Ar and silicon is extremely small.[12,13] For bombardment to an ion fluence higher than 10^{18}/cm^2, the defects in ion-bombarded silicon have been shown to be dominated by the void type.[5,8] The Ar incorporation probability will also surpass the quasisaturation regime[12,13] and increase with further increase in the fluence. This phenomenon is interpreted as the formation of Ar bubbles inside the void defects. The bubbles were formed initially by filling of the incorporated Ar into the void defects created by high fluence bombardment. The Ar inside the voids was overpressured due to contraction of the local silicon lattice around the voids, resulting in the solidification of the gas state Ar.[42,43] Such an interpretation has been supported by transmission electron microscopy (TEM).[8] For bombardment to a medium fluence ($\sim 10^{16}$/cm^2), it was believed[44,45] that most of the incorporated Ar is trapped at vacancy sites, thereby forming Ar-vacancy complexes while interstitial-type defects for Ar were negligible. In addition, much of the trapped Ar for the room temperature bombardment was immobile. Subsequently, aggregation of the atomically dispersed Ar and the chance of forming Ar bubbles should be small.[12,13] Nevertheless, controversial reports are found in the literature. Revesz *et al.*[46] observed Ar bubbles with an average diameter of 170 Å in 200 keV Ar-bombarded amorphous silicon to a fluence of 6 × 10^{15}/cm^2 using TEM, while Faraci *et al.*[43] reported the formation of Ar bubbles in 40 keV Ar-bombarded silicon single crystals to a fluence of 10^{16}/cm^2 at room temperature. Based on the fitting of the observed time-of-flight data, van Veen *et al.*[14] even argued that Ar clustering might take place at a fluence of 10^{14}/cm^2 for an ion energy of 3 keV. Conversely, Sawyer *et al.*[8] observed no Ar bubbles in their 1 keV Ar-bombarded silicon samples for ion fluences smaller than 10^{18}/cm^2; the Filius *et al.* data[12] also suggested that, for bombardment at a fluence of 10^{16}/cm^2, no Ar bubbles should be formed since the observed Ar desorption temperature was rather low.

Figure 9(a) shows the Ar K edge EXAFS spectra for 1 keV Ar-bombarded Si(100) to an ion fluence of 10^{16}/cm^2 and Fig. 9(b) is the Fourier transform of the corresponding EXAFS data shown in Fig. 9(a). The Ar-Ar nearest
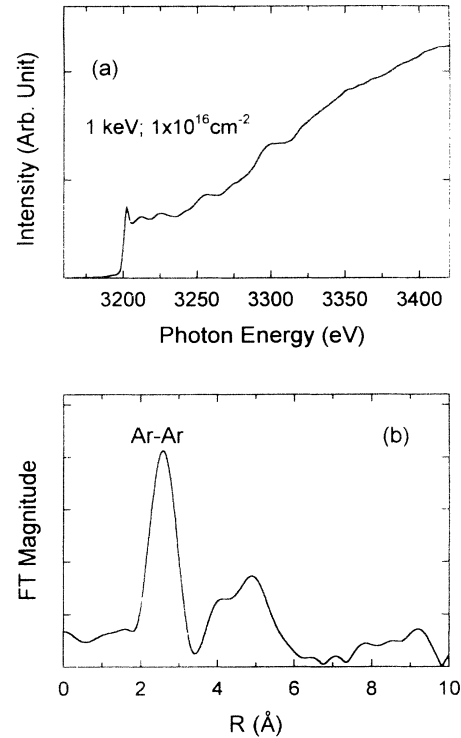

FIG. 9. (a) The Ar K EXAFS spectra for 1 keV Ar-bombarded Si(100) to an ion fluence of 1×10^{16}/cm^2. (b) The Fourier transformation of the corresponding EXAFS data shown in (a).

neighbor distance calculated by filtering and backtransforming the FT data was 2.96±0.05 Å. Since there are no experimental data for calibration of the measured phase shift, the theoretical data by Rehr *et al.*[47] were used in the present calculation. This value for the Ar-Ar nearest neighbor distance is larger than that of 2.84 Å in the 40 keV Ar-bombarded silicon but smaller than the 3.26 Å characteristic for solid Ar.[43] Moreover, the FT data in Fig. 9(b) showed no obvious shells for higher order nearest neighbors other than the second and hence are qualitatively different from those reported for the 40 keV Ar-bombarded silicon sample, where the FT data showed the "features for a fcc crystal."[43] The lack of long range ordering in our data [Fig. 9(b)] suggested that formation of solid Ar or Ar bubbles was unlikely at the present experimental conditions (0.5–1.5 keV with ion fluences up to 10^{16}/cm^2). However, the observed of Ar K edge data indicated that the incorporated Ar should have existed in some cluster form, otherwise no neighboring distance could be measured. By assuming that these Ar clusters in the bombarded layer were homogeneously distributed, the areal density could be estimated using the measured nearest neighbor distance, which yielded a value of 1.1 × 10^{15}/cm^2 and is in good agreement with the MEIS result. In addition, we found that the Ar concentration decreased to < 5 × 10^{13}/cm^2 after annealing to a temperature of 700 °C in all the samples in this study (see Sec. III H). Such a temperature is substantially lower than the Ar bubble desorption temperature. We concluded that

no Ar bubbles had been formed in the bombarded samples.

E. Damage depth profiling by variable-energy positron beam

In high-energy ($\sim 10^2$ keV) ion-induced amorphization, it has been proposed[48,49] that the interface between the amorphous layer and the crystalline substrate were populated with extended defects, which has been confirmed by TEM.[49] Based on the RBS data, Bean et al.[5] suggested that appreciable disorder and retained Ar existed below the surface to depths up to 500 Å for the 1 keV Ar-bombarded silicon at an elevated temperature of 800 °C. This depth is at least 10 times deeper than that predicted by TRIM or by Lindhard-Scharff-Schiott (LSS) theory.[50] The discrepancy was interpreted by Ar channeling during the bombardment. Since the resolution of RBS data is very poor, such a postulation needs further verification. In a recent paper, Al-Bayati et al.[9] used MEIS to measure the depth of Ar penetration in 510 eV Ar-bombarded c-Si. Although the Ar scattering peak overlapped with that of silicon, they found a depth of only 47 Å. They suggested that channeling was not an important factor but rather that Ar diffusion and defect stabilization played crucial roles. Our mass-resolved MEIS data showed that the retained Ar was located no deeper than 50 Å (Figs. 5 and 8). Although the depth resolution is determined by the energy resolution of the spectra, all calculations of the *linear* depth from MEIS or RBS data (which yield areal densities) depend on a knowledge of the volume density of the material. In our calculation, the density of the c-Si is used to approximate the true density of the bombarded layer. Such an approximation may underestimate the linear depth because the density for the defective silicon may be slightly lower than that of c-Si, but at most by a factor of 2. Therefore the depth for the retained Ar cannot exceed 100 Å. The extended defect layer, however, could be deeper owing to the effects of collision cascades. This effect could be seen partially from the dechanneling in the MEIS spectra, which could be interpreted as arising from extended defects with a relatively low density. In addition, MEIS has a detection limit of $\sim 5 \times 10^{13}/\text{cm}^2$. To have a better knowledge of the depth distribution of possible extended defects, we employed variable-energy positron-annihilation spectroscopy to profile the defect depth distribution. Positron-annihilation spectroscopy is especially sensitive to defects in solids[51] and it has been shown recently by the present authors[52] that it can be used to study defect profiling in ultrathin films. Figure 10 shows the positron-annihilation line-shape S parameters as a function of the mean positron implantation depth. The solid lines are fitted data which will be addressed in the following discussion. The mean positron penetration depth $\bar{z}$ (nm) depends on the positron energy E (keV), and can be calculated by[51]

$$\bar{z} = (A/\rho)E^n, \qquad (3.4)$$

where A is a constant having the value ~ 40 and the index n was chosen to be 1.6.[25,51] The line-shape S parameters
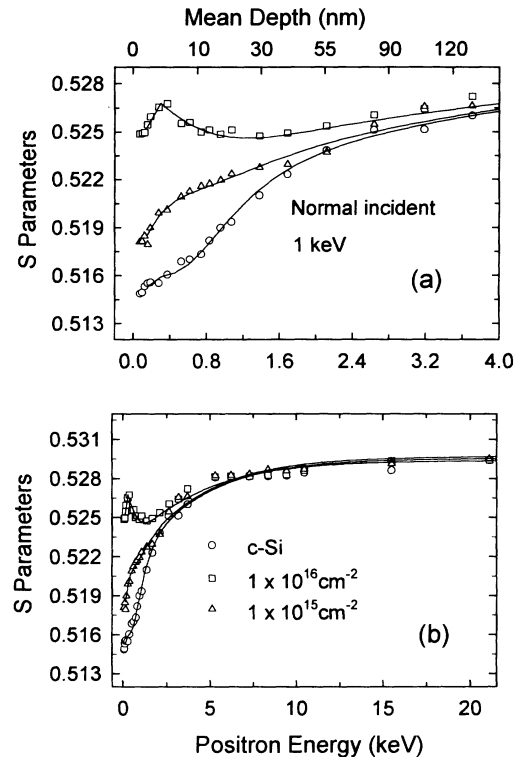

FIG. 10. Positron-annihilation line-shape S parameters vs mean positron implantation depth. (a) and (b) show different implantation depth scales. The data fits using a positron diffusion model are shown by the solid lines.

shown in Fig. 10 are similar to those for vacancy-type defects in semiconductors[53,54] and hence the positron results agree with the earlier conclusion that the majority of the ion-induced defects are of vacancy type. The depth for the defect structure shown in the figure was ~ 300 Å, which is substantially deeper than those measured from the MEIS data. However, the substantial differences in the S parameters seen in the figure are located in the top ~ 100 Å. In order to obtain more information from the positron results, the data were fitted using a positron diffusion model.[53] We assumed a model consisting of a four-layer structure where each layer had a different defect concentration: the top SiO_2 cap layer (10 Å) was followed by the ion-bombarded layer (50 Å), and then a 150 Å interface layer, followed by the c-Si substrate. The best fit was obtained by adjusting the layer thicknesses. Figure 11 shows the defect trap fraction for the four layers for the sample bombarded by 1 keV Ar to an ion fluence of $10^{16}/\text{cm}^2$. In the above fitting process, we found that it was necessary to introduce this "interface layer" with an atomic defect density approximately two orders of magnitude less than that in the bombarded layer in order to obtain a reasonable fit to the data. This result supports the existence of a transition layer with extended defects between the c-Si substrate and the bombarded layer, but the total thickness of the defect "layers" observed in the present work is at least 200 Å thinner than that reported by Bean et al.[5] and 700 Å thinner than those measured by photolumines-
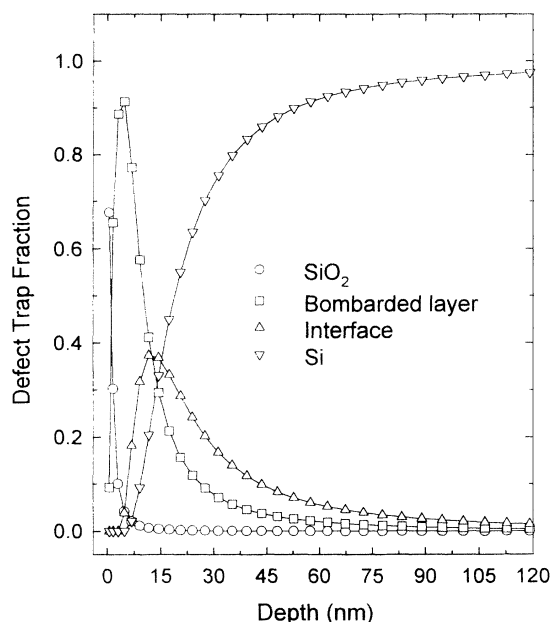
FIG. 11. The defect trap fraction vs mean positron implantation depth. The results were obtained by fitting using the four-layer structure model.

cence (PL) spectroscopy.[8] It should also be pointed out that using positron-annihilation spectroscopy to study the near-surface structure of solids is a relatively new topic. The behavior of positron diffusion, backdiffusion in the near-surface region, and the surface effects of the near-surface defect structure on the positron diffusion length are not well established. The interpretation of the data, e.g., the parameters used to calculate the depth scale, therefore needs more experimental and theoretical study. However, the preliminary results presented here are encouraging.

F. Bombardment-induced silicon carbide formation

In addition to the inherent disordering of the c-Si lattice, Ar bombardment also causes a dynamic ion-mixing process. On the one hand, foreign surface atoms and silicon atoms will be sputtered from the substrate at a sputtering rate about 0.8 to 1 for the 1 keV bombardment while the front of the ion-induced defects moves deeper into the subsurface region.[4] On the other hand, dynamic ion mixing will lead to the possibility of forming metastable structures by mixing the foreign atoms at the surface with the substrate silicon atoms. Among the possible mixing products, silicon carbide is believed to be another inherent structure that will be induced by Ar bombardment.[9,16–18] However, quantitative characterization of such a silicon carbide phase is difficult. The amount of the carbide phase formed is expected to be only of the order of a monolayer since the foreign atoms on a "clean" silicon surface should not be more than a few monolayers; as well, ion bombardment will also effectively sputter off the contaminants. One of the

most comprehensive studies of carbide formation by low-energy ion bombardment was performed by Al-Bayati *et al.*[9] using MEIS. Those experiments, however, showed only indirectly the existence of a silicon carbide phase by assuming that the additional ion scattering intensity at the interface of the disordered silicon peak was due to carbide formation. Also, these intensities were shown to be responsible for an additional disordering depth of ~10 Å, which was difficult to identify with the small number of foreign surface atoms. Another disadvantage of ion scattering in the analysis of carbide formation is that it is unable to distinguish between different chemical environments of the materials, resulting in difficulties in distinguishing the carbide from other species. More conventional surface analytical methods[16–18,55] using electron energy loss spectroscopy (EELS), AES, and secondary ion mass spectroscopy (SIMS) are also qualitative or are observed from carbide formed by dosing carbon on clean c-Si surfaces through high-temperature diffusion, which could be qualitatively different from that of ion-induced phase formation.[9]

In this study, we used XPS to measure the formation of bombardment-induced carbide as photoemission is crucially dependent on the chemical structure of solids. In order to clarify the relation between carbide formation and the number of foreign surface atoms, especially adventitious hydrocarbons, we used two cleaning approaches in the measurements. In the first approach, the as-received sample was cleaned in a 5% HF solution and then immediately loaded into the XPS analytical chamber which maintained a vacuum of 5×10^{-9} Torr. In the second approach, the HF-etched sample was ozone oxidized in a uv-light-induced ozone reaction chamber for 15 min and then 5% HF was used to remove the oxides; the process was repeated once again to further decrease the amount of adventitious surface hydrocarbons.[56] Figure 12 shows the high-resolution XPS C 1s spectra showing the formation of the carbide phase at the silicon near-surface by 1 keV Ar bombardment to various ion fluences. Figure 12(a) was measured for as-cleaned c-Si(100) and Figs. 12(b), 12(c), 12(d), and 12(e) were measured for the sample bombarded *in situ* in the XPS analytical chamber to ion fluences of $10^{15}/cm^2$, $5 \times 10^{15}/cm^2$, $10^{16}/cm^2$, and $2 \times 10^{16}/cm^2$, respectively. The initial coverage of the hydrocarbon on the surface before bombardment [Fig. 12(a)] was ~0.9 monolayer ($\sim 10^{15}/cm^2$) calculated using Eq. (3.1) where all the parameters for SiO_2 are replaced by those of hydrocarbon. This coverage could come from air exposure during the sample loading procedure. By bombardment to a fluence of $10^{15}/cm^2$ [Fig. 12(b)], a shoulder fitted to a peak at ~283.6 eV was observed. The relative intensity of this peak to that of the C-H peak increased with the ion fluence while its binding energy shifted downwards to 283 eV at a fluence of $10^{16}/cm^2$. The results clearly showed the formation of a carbide phase in the bombarded near-surface layer. The shift of its binding energy suggested that the carbide induced by lower fluence bombardment was of a metastable structure or a silicon-depleted phase. Bombardment to a higher fluence yielded the stabilization of the carbide phase through continuous ion mixing. Fur-
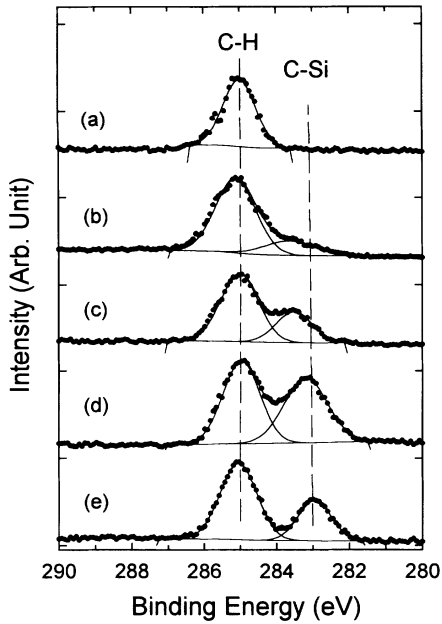
FIG. 12. XPS C $1s$ spectra showing the formation of SiC at different ion fluences: (a) as cleaned; bombarded to an ion fluence of (b) $1\times10^{15}/cm^2$, (c) $5\times10^{15}/cm^2$, (d) $1\times10^{16}/cm^2$, and (e) $2\times10^{16}/cm^2$.

ther increase in the bombardment fluence only resulted in a slight change in the relative intensities between C-H and C-Si. Calculation of the total amount of the carbide phase (Fig. 13) with the increase of the bombardment fluences indicated that the amount of the carbide phase increased with increasing ion fluences up to $10^{15}/cm^2$, which was approximately the critical fluence at which the c-Si phase was transformed into a disordered structure in
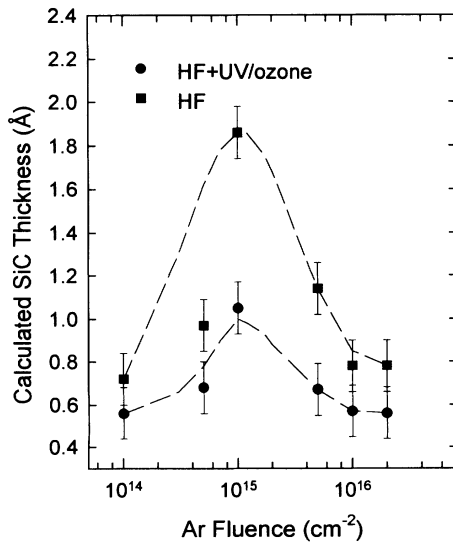
the near-surface layer (see Fig. 2). The amount of the carbide phase decreased with further increase of the fluence. This change was probably due to the competition between the sputtering and the stabilization of the carbide phase since no change of either the peak position or the total amount of the carbide phase was observed when the fluence was above $10^{16}/cm^2$. A dynamic equilibrium was likely achieved because the carbon was supplied by the chamber at a constant rate of ~0.005 monolayer/s (for the vacuum of $\sim5\times 10^{-9}$ Torr). In our bombardments, it took about 180 s to deliver 10^{15} Ar^+/cm^2 to a 100 mm^2 sample area (10 mm×10 mm). This will enable ~0.9 monolayer carbon to arrive at the sample surface. The equilibrium thickness of the carbide phase was ~0.8 Å for both cleaning approaches employed in this study (Fig. 13).

G. Depth profiling of the ion-induced silicon carbide

Previous studies[9],[18] suggested that the carbide phase were formed at the interface between the bombarded defect layer and c-Si substrate, which implied that the carbon had to diffuse through the defect layer without reacting with the silicon defects. However, interfacial carbide-induced dechanneling[9] was difficult to observe in the MEIS data. To reveal the carbide depth distribution in the bombarded near-surface layer, ARXPS was used to measure the location of the carbide phase. Figure 14 shows ARXPS C $1s$ spectra for 1 keV Ar-bombarded silicon to a fluence of $10^{16}/cm^2$. The polar angle is defined as the angle between the sample normal and the axis of the entrance of the electron energy analyzer. By changing the polar angle θ the detected photoemission intensity I_d
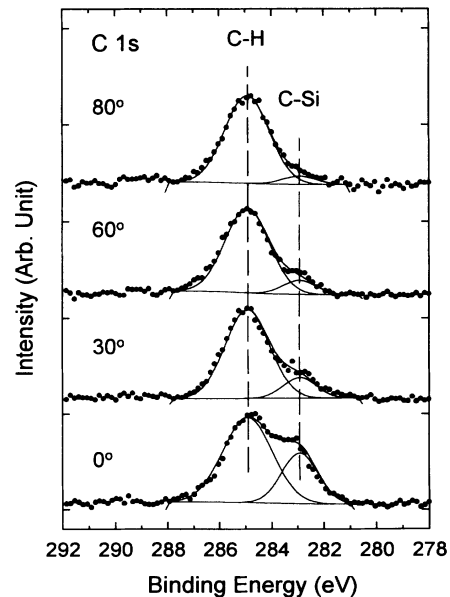

FIG. 13. Calculated SiC thickness for the samples bombarded to different ion fluences and different precleaning methods.

FIG. 14. Polar-angle-dependent XPS C $1s$ spectra for 1 keV argon-bombarded silicon to a fluence of $1\times10^{16}/cm^2$, showing that the silicon carbide phase was located at silicon subsurface.

will vary according to

$$I_d = I_e \exp[-t/(\lambda \cos \theta)], \qquad (3.5)$$

where I_e is the photoemission intensity from a chemical phase located at a distance t below the surface and λ is the inelastic mean free path. This enables us to define an effective sampling depth, $t_{\text{effective}} = \lambda \cos \theta$, at which 63% of the photoemission does not undergo inelastic scattering. Therefore, by increasing the polar angle, the measurement will become more surface sensitive. One sees from Fig. 14 that the carbide intensity decreases with increase of the polar angle, thereby suggesting that the carbide was indeed located at the subsurface. The hydrocarbon was clearly located at the surface since there is almost no change in the photoemission intensity for the peak at 285 eV as a function of θ. However, since the maximum $t_{\text{effective}}$ could not go deeper than 40 Å, the XPS might not be able to detect enough photoemission at the interface. We then applied the "ultrashallow depth profiling" technique,[20,57] which was recently developed, to verify the results obtained from ARXPS. Briefly, in this technique, the controlled removal of 5 Å silicon was accomplished by uv ozone oxidation of the silicon followed by HF etching to remove the oxide, and by immediately transferring the sample into an analytical instrument, e.g., in XPS. The depth profiling with a resolution of $\sim$5 Å was achieved by sequential silicon removal and XPS measurement. In this study, the interface between the bombarded defect layer and the c-Si substrate was determined by watching the Si $2p$ spectra, in which no photoemission from silicon dangling bonds could be observed from an oxidized c-Si sample at large polar angles (e.g., 80°), and by comparing the full width at half maximum (FWHM) of Si $2p_{3/2}$ with that of c-Si. The depth profiling data are shown in Fig. 15 and the results from ARXPS are also included for comparison. Similar to
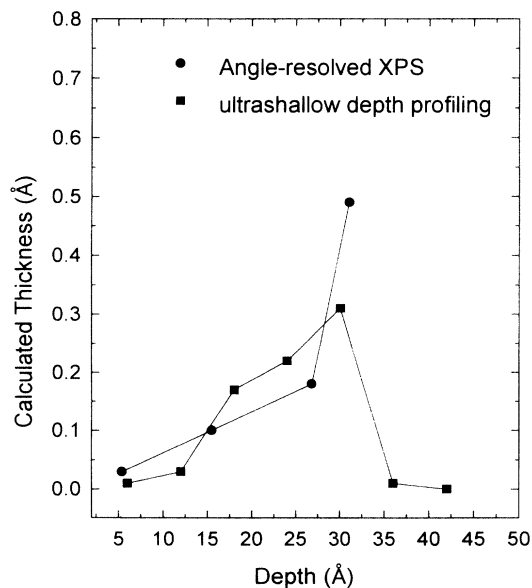
the calculation of the depth from the MEIS spectra, the determination of the depth in the present technique also depends on a knowledge of the density for the disordered silicon. The c-Si density was used as an approximation in the present calculation. Hence, the depth shown in the figure may underestimate the linear depth since the density of the disordered Si could be smaller than that of c-Si. However, while no silicon carbide phase could be observed in the ultrashallow depth profiling, XPS still detected the silicon dangling bonds. This indicated that the profile had not yet reached to the interface. The carbide phase therefore should not be located at the interface, but rather inside the defect layer. This conclusion seemed more plausible since the probability of ion mixing inside the bombarded layer is much larger than that at the interface. The total amount of the carbide phase measured by these two techniques was approximately the same, i.e., $\sim$0.8 Å. This rather small number suggested that the carbide phase was most probably dispersed inside the bombarded layer and carbon was bonded to silicon at localized defect sites. The chance to form large crystallite silicon carbide phase would be very small.

H. Recrystallization of the disordered near-surface layer

One of the key issues for surface cleaning by Ar bombardment is to restore long range order in the bombarded near-surface layer through epitaxial recrystallization. Early work by Seidel *et al.*,[58] however, indicated that the Ar incorporated in the 200 keV bombarded silicon had a strong inhibiting effect on recrystallization by postannealing. Yamada *et al.*[10] also showed that recrystallization could not be achieved through postannealing up to 750 °C for Ar-bombarded silicon at ion energies higher than 1 keV. For 1 keV bombardment, recrystallization was only marginally achieved when the ion fluence was below $5 \times 10^{15}/\text{cm}^2$. The results obtained from an alternative approach using bombardment at an elevated temperature, however, indicated that recrystallization could be realized only when the bombardment energy was low enough[11] not to introduce extended defects.[5,9] The failure of recrystallization has been interpreted as evidence for ion-induced enhanced defect migration and stabilization.[5,11] It is therefore of importance to accurately measure the Ar redistribution and defect migration upon annealing.

Figure 16 shows the MEIS depth profile of the Ar redistribution after a 500 °C anneal for 30 min for a Si(100) sample bombarded with 0.5 keV Ar to an ion fluence of $10^{16}/\text{cm}^2$. The solid line is the theoretical fit to a Gaussian function. The measured Ar areal densities for the as-bombarded and the annealed sample are 8.3 $\times 10^{14}/\text{cm}^2$ and 5.4 $\times 10^{14}/\text{cm}^2$, respectively. The amount of desorbed Ar over that of the as-bombarded sample at this temperature was then $\sim$35%. The profile clearly showed that the desorption occurred from the surface region. The annealing led to a change of the distribution from an asymmetric to a symmetric Gaussian shape. The appreciable Ar retention could certainly serve as a barrier

FIG. 15. Depth distribution of the silicon carbide phase measured by angle-resolved XPS and ultrashallow depth profiling technique.
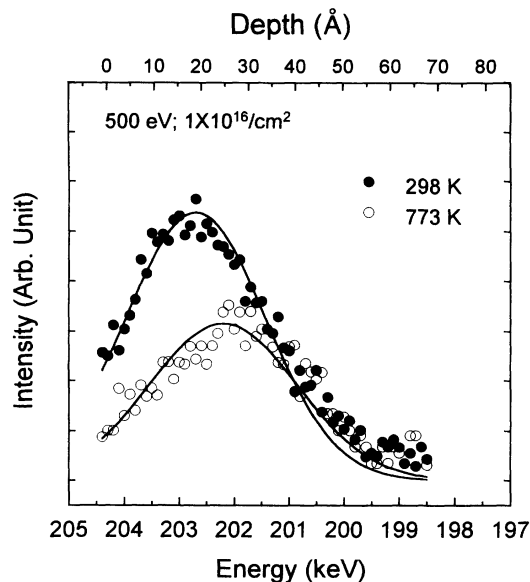
FIG. 16. Argon depth profile by MEIS shows the redistribution of argon after 773 K anneal for a Si(100) sample bombarded with 1 keV argon to an ion fluence of $1 \times 10^{16}/\text{cm}^2$.

for recrystallization at this temperature. In this study, it was found that a temperature of $\sim 700\,^\circ$C was required for desorption of the incorporated Ar to a level below the present detection limit ($< 10^{13}/\text{cm}^2$). Figure 17 shows the MEIS data for the change of the retained Ar con-
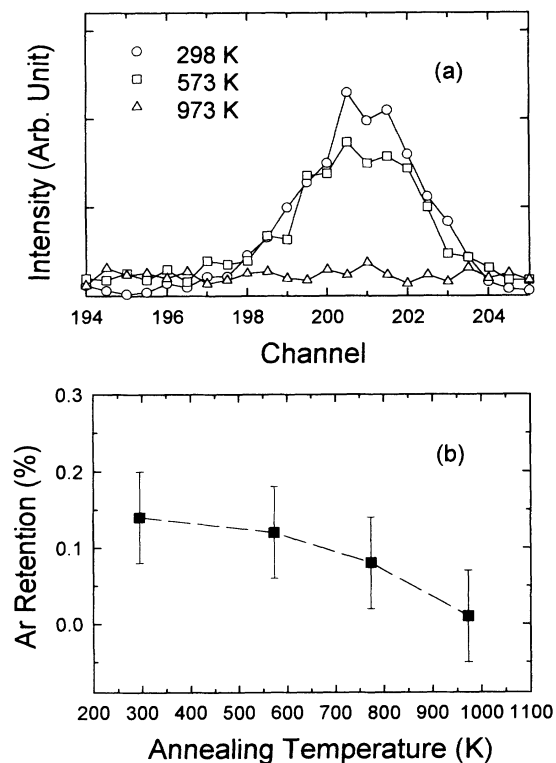
centration in the bombarded samples at different annealing temperatures. No Ar retention could be observed by MEIS after the bombarded samples were annealed in vacuum at 700 $^\circ$C for 30 min. The Ar concentration should then be lower than $10^{14}/\text{cm}^2$, which is the detection limit of MEIS. Further measurements by XPS also confirmed no photoemission of incorporated Ar after a 700 $^\circ$C anneal. The detection limit of Ar for XPS is $\sim 5 \times 10^{13}/\text{cm}^2$. We then concluded that almost all the incorporated Ar was desorbed at this temperature.

The structural changes upon annealing were monitored by XANES. Figure 18 shows the measured silicon L edge
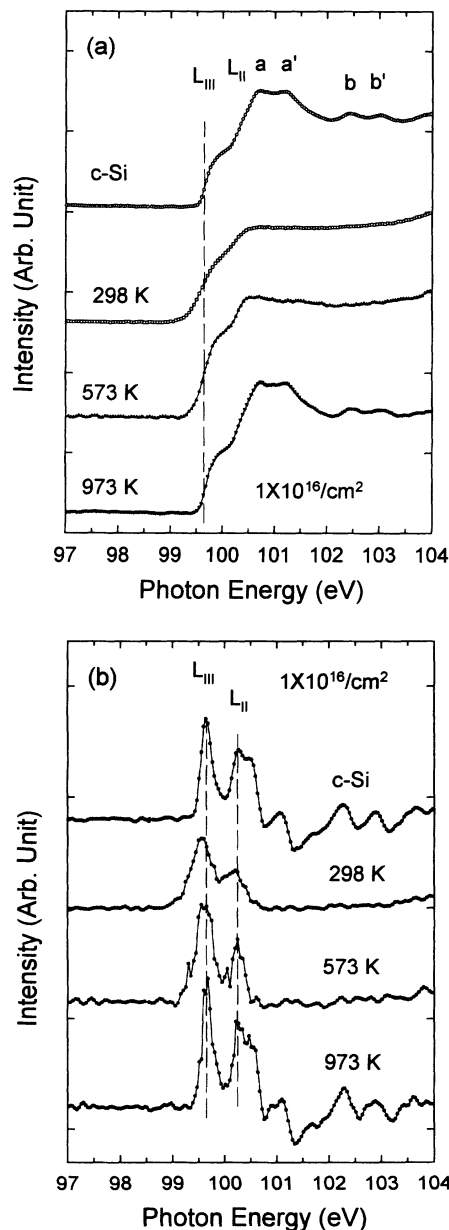

FIG. 17. (a) Change of argon intensities in 1 keV argon-bombarded Si(100) to an ion fluence of $1 \times 10^{16}/\text{cm}^2$ against different annealing temperatures. (b) Calculated argon retention with different annealing temperatures.

FIG. 18. (a) Si $L_{\text{II,III}}$ XANES spectra for HF-etched Si(100) and 1 keV argon-ion-bombarded Si(100) annealed to different temperatures as labeled in the figure. (b) The first order derivative of the Si $L_{\text{II,III}}$ XANES spectra for the corresponding spectra shown in (a).
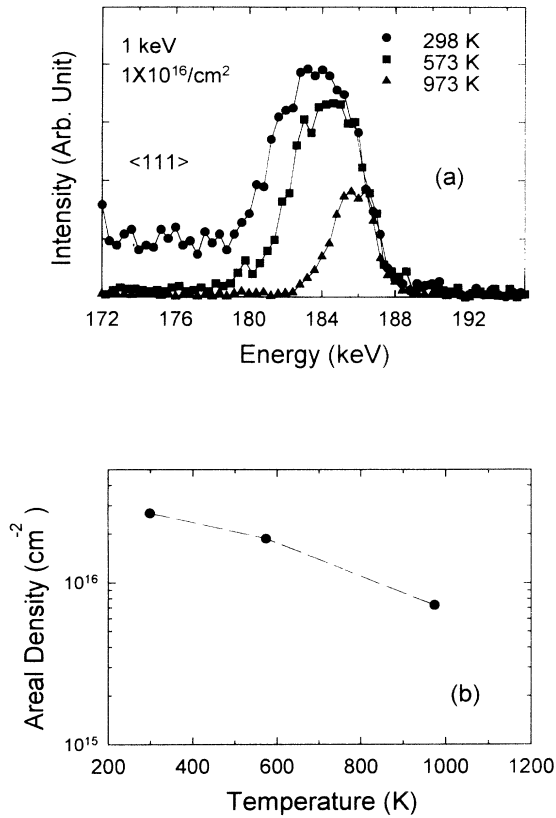
FIG. 19. MEIS spectra showing the silicon surface peaks for 1 keV bombarded Si(100) to an ion fluence of $1 \times 10^{16}/\mathrm{cm}^2$ and followed by postannealing at different temperatures.
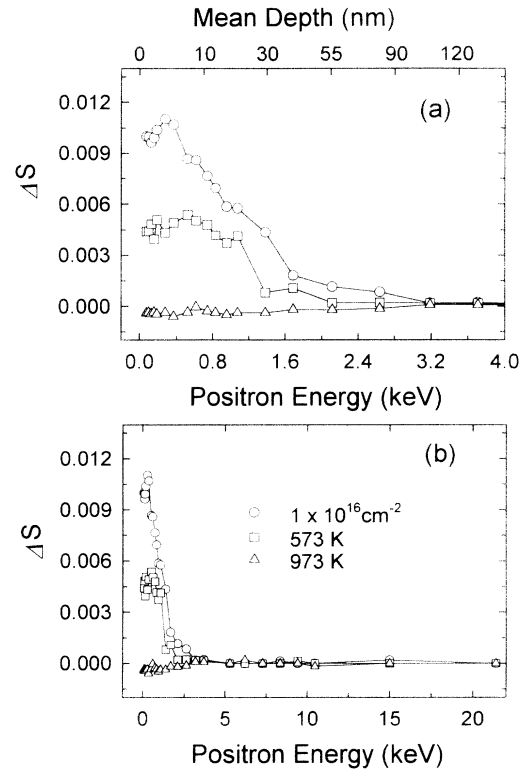

FIG. 20. Relative changes of positron line-shape parameters for 1 keV argon-bombarded Si(100) and subsequent annealed samples at 573 K and 973 K, respectively. (a) and (b) are plots at different positron implantation energies.

spectra and the first order derivatives for a sample bombarded by 1 keV Ar to a fluence of $10^{16}/\mathrm{cm}^2$ and subjected to anneal at different temperatures. The recovery of the long range order was clearly seen for the sample after a 700 °C anneal. Compared with that of c-Si, all the crystalline features were recovered. The evidence for epitaxial recrystallization can be seen in Fig. 19 where MEIS data reveal that at 700 °C (973 K), the areal concentration of the displaced silicon was $\sim 7.8 \times 10^{15}/\mathrm{cm}^2$, which was the same as that for c-Si in Fig. 4. Annealing at a lower temperature (573 K or 300 °C) only led to a slight decrease in the number of displaced silicon atoms. The recrystallization, however, was clearly epitaxial as evidenced by the interface movement shown in Fig. 19(a). The normalized thickness of the recrystallized silicon at 300 °C was ~ 12 Å.

Figure 20 shows the relative changes of positron line-shape parameter, $\Delta S = S_i - S_{c\text{-Si}}$, as functions of positron implantation energy for the bombarded and postannealed samples. After the 973 K (700 °C) anneal, no defects could be observed from the profiling. Since it has been shown[59] that positron-annihilation spectroscopy was sensitive to defects produced by 5 MeV silicon self-implantation to a fluence of $5 \times 10^{11}/\mathrm{cm}^2$, we concluded that the observed epitaxial layer was comparable to the defect-free c-Si.

IV. SUMMARY

In summary, we present a comprehensive study of the near-surface structure of silicon (100) modified by low-energy Ar bombardment using direct and nondestructive depth profiling and structural measurements for both displaced silicon and incorporated Ar at the subnanometer level. The structure and depth distribution of the silicon carbide formed in the dynamic mixing process were also identified. The results showed clearly that low-energy Ar bombardment can dramatically modify both the structural and electrical properties of the silicon near-surface layer by introducing structural defects and band-gap states. At the moderate bombardment fluence of $10^{16}/\mathrm{cm}^2$, the near-surface layer (up to ~ 50 Å) was completely amorphized while no Ar bubbles were observed. The distribution of the dispersed Ar could be approximated by a Gaussian function. Complete epitaxial recrystallization was achieved by postvacuum annealing at 700 °C for 30 min.

ACKNOWLEDGMENTS

[1] H. Winters and J. Coburn, Surf. Sci. Rep. **14**, 161 (1992).

[2] See, e.g., *Ion Beam Assisted Film Growth*, edited by T. Itoh (Elsevier, Amsterdam, 1989).

[3] See, e.g., *Practical Surface Analysis*, edited by D. Briggs and M.P. Seah (Wiley, Toronto, 1992).

[4] *Sputtering by Particle Bombardment II*, edited by R. Behrisch (Springer-Verlag, Berlin, 1983).

[5] J.C. Bean, G.E. Becker, P.M. Petroff, and T.E. Seidel, J. Appl. Phys. **48**, 907 (1977).

[6] H.E. Farbsworth, R.E. Schlier, T.H. George, and R.M. Burger, J. Appl. Phys. **29**, 1150 (1958)

[7] G. Magaritondo, J.E. Rowe, and S.B. Christman, Phys. Rev. B **14**, 5396 (1976).

[8] W.D. Sawyer, J. Weber, G. Nabert, J. Schmalzlin, and H.-U. Habermeier, J. Appl. Phys. **68**, 6179 (1990).

[9] A.H. Al-Bayati, K.G. Orrman-Rossiter, R. Badheka, and D.G. Armour, Surf. Sci. **237**, 313 (1990); A.H. Al-Bayati, K.G. Orrman-Rossiter, and D.G. Armour, *ibid.* **249**, 293 (1991).

[10] I. Yamada, D. Marton, and F.W. Saris, Appl. Phys. Lett. **37**, 563 (1980).

[11] J.H. Comfort, L.M. Garverick, and R. Reif, J. Appl. Phys. **62**, 3388 (1987).

[12] H.A. Filius, A. van Veen, K.R. Bijkerk, and J.H. Evans, Radiat. Eff. **108**, 1 (1989).

[13] W.M. Lau, I. Bello, L.J. Huang, X. Feng, M. Vos, and I.V. Mitchell, J. Appl. Phys. **74**, 7101 (1993).

[14] G.N.A. van Veen, F.H.M. Sanders, J. Dieleman, A. van Veen, D.J. Oostra, and A.E. de Vries, Phys. Rev. Lett. **57**, 739 (1985).

[15] R.G. Elliman, J.S. Williams, W.L. Brown, A. Leiberich, D.M. Maher, and R.V. Knoell, Nucl. Instrum. Methods Phys. Res. Sect. B **19/20**, 435 (1987).

[16] W.M. Skiff, R.W. Carpenter, and S.H. Lin, J. Appl. Phys. **62**, 2439 (1987).

[17] H. Froitzheim, U. Kohler, and H. Lammering, Phys. Rev. B **30**, 5771 (1984).

[18] M.J. Kim and R.W. Carpenter, J. Mater. Res. **5**, 347 (1990).

[19] L.J. Huang and W.M. Lau, Appl. Phys. Lett. **60**, 1108 (1992), and references therein.

[20] W.M. Lau, L.J. Huang, W.H. Chang, M. Vos, and I.V. Mitchell, Appl. Phys. Lett. **63**, 78 (1993).

[21] M. Vos and I.V. Mitchell, Phys. Rev. B **45**, 9398 (1992).

[22] M. Kasrai, M.E. Fleet, G.M. Bancroft, K.H. Tan, and J.M. Chen, Phys. Rev. B **43**, 1763 (1991).

[23] B.X. Yang, F.H. Middelton, B.G. Olsson, G.M. Bancroft, J.M. Chen, T.K. Sham, K.H. Tan, and D.J. Wallace, Nucl. Instrum. Methods Phys. Res. Sect. A **316**, 422 (1992).

[24] P.J. Schultz, Nucl. Instrum. Methods Phys. Res. Sect. B **30**, 94 (1988).

[25] L.J. Huang, W.M. Lau, P.J. Simpson, and P.J. Schultz, Phys. Rev. B **46**, 4086 (1992).

[26] S. Tanuma, C.J. Powell, and D.R. Penn, Surf. Interface Anal. **17**, 927 (1991).

[27] M. Nakazawa, Y. Nishioka, H. Sekiyama, and S. Kawase, J. Appl. Phys. **65**, 4019 (1989).

[28] F.C. Brown and O.P. Rustgi, Phys. Rev. Lett. **28**, 497 (1972).

[29] G.R. Harp, Z.L. Han, and B.P. Tonner, J. Vac. Sci. Technol. A **8**, 2566 (1990).

[30] A. Bianconi, Surf. Sci. **89**, 41 (1979); A. Bianconi and R.S. Bauer, *ibid.* **99**, 76 (1980).

[31] M. Kasrai, Z. Yin, and G.M. Bancroft, J. Vac. Sci. Technol. A **11**, 2694 (1993).

[32] L.J. Huang and W.M. Lau, J. Vac. Sci. Technol. A **10**, 812 (1992).

[33] F.J. Himpsel, B.S. Meyerson, F.R. McFeely, J.F. Morar, A. Taleb-Ibrahimi, and J.A. Yarmoff, in *Photoemission and Absorption Spectroscopy of Solids and Interfaces with Synchrotron Radiation*, Proceedings of the International School of Physics "Enrico Fermi," Course 108, Varenna, 1988, edited by M. Campagna and R. Rosei (North-Holland, Amsterdam, 1990), p. 203.

[34] B.K. Agarwal, *X-ray Spectroscopy* (Springer-Verlag, Berlin, 1991).

[35] P.A. Lee, P.H. Citrin, P. Eisenberger, and B.M. Kincaid, Rev. Mod. Phys. **53**, 769 (1981).

[36] M. Kasrai (unpublished).

[37] W.K. Chu, J.W. Mayer, and M.-A. Nicolet, *Backscattering Spectroscopy* (Academic Press, New York, 1978).

[38] L.C. Feldman, I. Stensgaard, P.J. Silverman, and T.E. Jackman, in *Proceedings of the International Conference on Physics of SiO$_2$ and Its Interfaces*, edited by S.T. Pantelides (Pergamon Press, Oxford, 1978).

[39] P. Rabinzohn, G. Gautherin, B. Agius, and C. Cohen, J. Electrochem. Soc. **131**, 905 (1984).

[40] S. Kostic, D.G. Armour, and G. Carter, in *Materials Modification by High-Fluence Ion Beams*, edited by R. Kelly and M. Fernanda da Silva (Kluwer, Dordrecht, 1989), p. 237.

[41] J.F. Ziegler, and J.P. Biersack, *The Stopping and Range of Ions in Solids* (Pergamon Press, New York, 1975).

[42] J.H. Evans and D.J. Mazey, Scr. Metall. **19**, 621 (1985).

[43] G. Faraci, S. La Rosa, A.R. Pennisi, S. Mabilio, and G. Tourillon, Phys. Rev. B **43**, 9962 (1991); G. Faraci, in *Fundamental Aspects of Inert Gases in Solids*, edited by S.E. Donnelly and J.H. Evans (Plenum Press, New York, 1991), p. 251.

[44] J. Bourgoin and M. Lannoo, *Point Defects in Semiconductors II* (Springer-Verlag, Berlin, 1983).

[45] G.D. Watkins and J.R. Troxell, Phys. Rev. Lett. **44**, 593 (1980).

[46] R. Revesz, M. Wittmer, J. Roth, and J.W. Mayer, J. Appl. Phys. **49**, 5199 (1978).

[47] J.J. Rehr, J. de Leon, and S.I. Zabinsky, J. Am. Chem. Soc. **113**, 5135 (1991).

[48] L. Csepregi, E.F. Kennedy, S.S. Lau, J.W. Mayer, and T.W. Sigmon, Appl. Phys. Lett. **29**, 645 (1976).

[49] L.D. Glowinski, K.N. Tu, and P.S. Ho, Appl. Phys. Lett. **28**, 312 (1976).

[50] J. Lindhard, M. Scharff, and H. Schiott, K. Dan. Vidensk.

Selsk. Mat.-Fys. Medd. **33**, 1 (1963).

[51] P.J. Schultz and K.G. Lynn, Rev. Mod. Phys. **60**, 701 (1988).

[52] L.J. Huang, R.W.M. Kwok, W.M. Lau, H.T. Tang, W.N. Lennard, I.V. Mitchell, and P.J. Schultz, Appl. Phys. Lett. **62**, 163 (1993).

[53] G.W. Rubloff, B. Nielson, K.G. Lynn, D.O. Welch, and T.C. Leung, Vacuum **41**, 790 (1990).

[54] P.J. Schultz, E. Tandberg, K.G. Lynn, B. Nielsen, T.E. Jackman, M.W. Denhoff, and G.C. Aers, Phys. Rev. Lett.

61, 187 (1988).

[55] Y.H. Xie, K.L. Wang, and Y.C. Kao, J. Vac. Sci. Technol. A **3**, 1035 (1985).

[56] J.R. Vig, J. Vac. Sci. Technol. A **3**, 1027 (1985).

[57] W.H. Chang, L.J. Huang, W.M. Lau, M. King, and T. Abraham, Appl. Phys. Lett. **64**, 2154 (1994).

[58] T.E. Seidel, R.L. Meek, and A.G. Cullis, J. Appl. Phys. **46**, 600 (1975).

[59] B. Nielsen, O.W. Holland, T.C. Leung, and K.G. Lynn, J. Appl. Phys. **74**, 1636 (1993).